BULLETIN OF THE POLISH ACADEMY OF SCIENCES
TECHNICAL SCIENCES
Vol. 52, No. 1, 2004

The progress of nanocrystalline hydride electrode materials

M. JURCZYK*

Institute of Materials Science and Engineering, Poznań University of Technology, Sklodowska-Curie 5 Sq., 60-965 Poznań, Poland

Abstract. This paper reviews research at the Institute of Materials Science and Engineering, Poznań University of Technology, on the synthesis of nanocrystalline hydride electrode materials. Nanocrystalline materials have been synthesized by mechanical alloying (MA) followed by annealing. Examples of the materials include TiFe-, ZrV_2-, $LaNi_5$ and Mg_2Ni-type phases. Details on the process used and the enhancement of properties due to the nanoscale structures are presented. The synthesized alloys were used as negative electrode materials for Ni-MH battery. The properties of hydrogen host materials can be modified substantially by alloying to obtain the desired storage characteristics. For example, it was found that the respective replacement of Fe in TiFe by Ni and/or by Cr, Co, Mo improved not only the discharge capacity but also the cycle life of these electrodes. The hydrogen storage properties of nanocrystalline ZrV_2- and $LaNi_5$-type powders prepared by mechanical alloying and annealing show no big difference with those of melt casting (polycrystalline) alloys. On the other hand, a partial substitution of Mg by Mn or Al in Mg_2Ni alloy leads to an increase in discharge capacity, at room temperature. Furthermore, the effect of the nickel and graphite coating on the structure of some nanocrystalline alloys and the electrodes characteristics were investigated. In the case of Mg_2Ni-type alloy mechanical coating with graphite effectively reduced the degradation rate of the studied electrode materials. The combination of a nanocrystalline TiFe-, ZrV_2- and $LaNi_5$-type hydride electrodes and a nickel positive electrode to form a Ni-MH battery, has been successful.

Keywords: nanocrystalline materials, hydrogen absorbing materials, electrode materials, Ni-MH_x batteries.

1. Introduction

An interest in the study of nanostructured materials has increased, recently. This is due to recent advances in materials' synthesis and characterization techniques and the realization that these materials exhibit many interesting and unexpected physical as well as chemical properties with a number of potential technological applications. For example, hydrogen storage nanomaterials are the key to the future of the storage and batteries/cells industries [1–4].

The TiFe, ZrV_2 and $LaNi_5$ phases are familiar materials which absorb large quantities of hydrogen under mild conditions of temperature and pressure. These types of hydrogen forming compounds have been recently proven to be very attractive as negative electrode material in rechargeable nickel-metal hydride batteries [3]. Unlike the conventional lead acid and nickel cadmium batteries, metal hydride batteries have a much lower content of environmentally toxic metals. The hydrogen storage materials combine a high reversible energy storage capacity with fast electrochemical activation, excellent long term cycling stability and good charge/discharge kinetics, making Ni-MH batteries nowadays a serious alternative for Ni-Cd batteries. Magnesium-based hydrogen storage alloys have been also considered to be possible candidates for electrodes in Ni-MH batteries.

The Ni-MH battery is a battery with a hydrogen storage alloy as its negative electrode, which is able to absorb and desorb reversibly a large amount of hydrogen at room temperature. The working principle of this battery is expressed by the following equation [3]:

$$\mathrm{Ni(OH)_2} + M \underset{\text{discharge}}{\overset{\text{charge}}{\leftrightarrow}} \mathrm{NiOOH} + \mathrm{MH}, \qquad (1)$$

where M stands for the hydrogen storage alloy and MH for metal hydride. The nickel-metal hydride battery has the following advantages: i) the cell voltage is almost the same as the value of a Ni-Cd battery, i.e. 1.2–1.3 V and ii) the cell can be charged and discharged at high rates and low temperatures.

TiFe and ZrV_2 alloys crystallize in the cubic CsCl and $MgCu_2$ structures and at room temperature they absorb up to 2 H/f.u. and 5.5 H/f.u., respectively. On the other hand, $LaNi_5$ alloy crystallizes in the hexagonal $CaCu_5$ structure and at room temperature can absorb up to 6 H/f.u. [5–7]. Nevertheless, the application of these types of materials in batteries has been limited due to slow absorption/desorption kinetics in addition to a complicated activation procedure. The properties of hydrogen host materials can be modified substantially by alloying to obtain the desired storage characteristics, e.g. proper capacity at a favourable hydrogen pressure [3,4]. TiFe alloy is lighter and cheaper than the $LaNi_5$-type material. To improve the activation of this alloy several approaches have been adopted. For example, the replacement of Fe by some amount of transition metals to form secondary phase may improve the activation properties of TiFe. On the other hand, the electrochemical activity of ZrV_2-type materials can be stimulated by substitution, in which Zr is partially replaced by Ti and V is partially replaced by other transition metals (Cr, Mn and Ni) [8, 9]. Independently, it was found that the respective replacement of La and Ni in $LaNi_5$ by small amounts of Zr and Al resulted in a prominent increase

* e-mail: jurczyk@sol.put.poznan.pl

in the cycle life time without causing much decrease in capacity [3, 10].

Magnesium-based alloys have been extensively studied recently, too [3, 11–13]. The polycrystalline Mg_2Ni alloy can reversibly absorb and desorb hydrogen only at high temperatures. Upon hydrogenation at 523 K, Mg_2Ni transforms into the hydride phase Mg_2NiH_4. Substantial improvements in the hydriding-dehydriding properties of Mg_2Ni metal hydrides could be possibly achieved by the formation of nanocrystalline structures [11]. The hydrogen content in Mg_2NiH_4 is also relatively high, being 3.6 wt%, whereas only 1.5 wt% in $LaNi_5H_6$.

Conventionally the metal hydride materials have been prepared by arc melting and annealing. Non-equilibrium processing techniques such as mechanical alloying or high–energy ball–milling (HEBM) can be utilised to synthesise highly activated nanocrystalline powders [2–4, 14]. These materials exhibit quite different properties from both crystalline and amorphous materials, due to structure, in which extremely fine grains are separated by what some investigators have characterized as „glass-like" disordered grain boundaries. The generation of new metastable phases or materials with an amorphous grain boundary phase offers a wider distribution of available sites for hydrogen and thus totally different hydrogenation behaviour. The mechanism of amorphous phase formation by MA is due to a chemical solid state reaction, which is believed to be caused by the formation of a multilayer structure during milling [15].

To be useful for storing hydrogen the hydride should: be capable of storing large quantities of hydrogen, be readily formed and decomposed, have reaction kinetics satisfying the charge-discharge requirements of the system, have the capability of being cycled without alteration in pressure-temperature characteristics during the life of the system, have low hysteresis, have good corrosion stability, have low cost, and be, at least, as safe as other energy carriers.

The main objective of the present paper is to review the advantages of some nanomaterials, their application in batteries and the challenges involved in their fabrication. In this work, the electrochemical properties of TiFe-, ZrV_2-, $LaNi_5$- and Mg_2Ni-type alloys are investigated. Details of the processing used and the enhancement of properties due to the nanoscale structures are presented. The measurements of the properties are also included. Then the effect of the nickel and graphite coating on the structure of some alloys and electrodes characteristics is studied. Finally, the electronic properties of nanocrystalline alloys with electrochemical behaviour of sealed Ni-MH batteries using nanocrystalline TiFe-type anodes are given.

2. Mechanical alloying

Mechanical alloying was developed in the 1970's as a technique for dispersing nanosized inclusions into nickel-based alloys [15]. During the last years, the MA process has been successfully used to prepare a variety of alloy powders including powders exhibiting supersaturated solid solutions, quasicrystals, amorphous phases and nano-intermetallic compounds [16]. MA technique has been proved as a novel and promising method for alloy formation, especially in the preparation of metal hydride materials [2, 4, 11, 14].

The raw materials used for MA are available as commercially high purity powders that have sizes in the range of 1–100 μm. During the mechanical alloying process, the powder particles are periodically trapped between colliding balls and are plastically deformed. Such a feature occurs because of the generation of a wide number of dislocations as well as other lattice defects. Furthermore, the ball collisions cause fracturing and cold welding of the elementary particles, forming clean interfaces at the atomic scale. Further milling leads to an increase of the interface number and the sizes of the elementary component area decrease from millimeter to submicrometer lengths. Concurrently to this decrease of the elementary distribution, some nanocrystalline intermediate phases are produced inside the particles or at its surfaces. As the milling duration develops, the content fraction of such intermediate compounds increases leading to a final product which properties are the function of the milling conditions.

3. Experimental

In 1996 a research program was initiated at Institute of Materials Science and Engineering, Poznań University of Technology in which fine grained, intermetallic compounds were produced by mechanical alloying or high energy ball milling [4, 8, 9, 13, 17–25]. The mechanical synthesis of nanopowders and their subsequent consolidation is an example of how the idea of nanostructured materials can be realized in alloys by so called bottom-up approach.

Conventionally the materials were prepared by arc melting of stoichiometric amounts of the constituent elements (purity 99.8% or better) in an argon atmosphere. The alloy lump was pulverized in few hydriding/dehydriding cycles to a fine powder ($\leqslant 45$ μm).

Another processing method, mechanical alloying was performed under argon atmosphere using a SPEX 8000 Mixer Mill. The purity of the starting materials was at least 99.8% and the composition of the starting powder mixture corresponded to the stoichiometry of the „ideal" reactions. The as-milled powders were heat treated at 723–1073 K for 0.5 h under high purity argon to form ordered phases (see text for details). The powders were characterized by means of X-ray diffraction (XRD) using a Co Kα radiation, at the various stages during milling, prior to annealing and after annealing. The crystallite sizes were estimated by Scherrer method as well as by atomic force microscopy (AFM) method.

The mechanically alloyed materials, in both amorphous and in nanocrystalline forms, as well as the con-

ventionally prepared materials (pulverized to a fine powder), with 10 wt% addition of Ni powder, were subjected to electrochemical measurements as working electrodes. A detailed description of the electrochemical measurements was given in Refs. [17, 18].

4. Results and discussion

The effect of MA processing was studied by X-ray diffraction, microstructural investigations as well as by electrochemical measurements. In the present study, TiFe-, ZrV_2-, $LaNi_5$- and Mg_2Ni-type alloys have been prepared by mechanical alloying (Fig. 1). Formation of these alloys was achieved by annealing the amorphous materials in high purity argon atmosphere (Table 1).

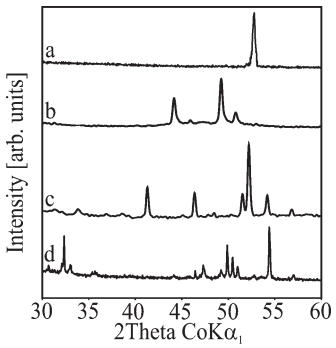

Fig. 1. XRD spectra of nanocrystalline TiFe (a), ZrV_2 (b), $LaNi_5$ (c) and Mg_2Ni (d) alloys produced by mechanical alloying followed by annealing (TiFe MA for 20 h and heat treated at 973 K for 0.5 h; ZrV_2 MA for 40 h and heat treated at 1073 K for 0.5 h; $LaNi_5$ MA 30 h and head treated at 973 K for 0.5 h; Mg_2Ni MA 90 h and head treated at 723 K for 0.5 h)

4.1. TiFe-type materials. Figure 2 shows a series of XRD spectra of mechanically alloyed Ti-Fe powder mixture (53.85 wt% Ti + 46.15 wt% Fe) subjected to milling at increasing time. The originally sharp diffraction lines of Ti and Fe gradually become broader (Fig. 2b) and their intensity decreases with milling time. The powder mixture milled for more than 20 h has transformed completely to the amorphous phase, without formation of other phase (Fig. 2c). During the MA process the crystalline size of the Ti decreases with mechanical alloying time and reaches a steady value of 20 nm after 15 h of milling. This size of crystallites seems to be favourable to the formation of an amorphous phase, which develops at the Ti-Fe interfaces. Formation of the nanocrystalline alloy TiFe was achieved by annealing the amorphous material in high purity argon atmosphere at 973 K for 0.5 h (Table 1). All diffraction peaks were assigned to those of CsCl-type structure with cell parameter $a = 0.2973$ nm. When nickel is added to $TiFe_{1-x}Ni_x$ the lattice constant a increases.

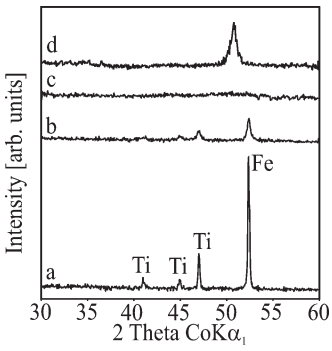

Fig. 2. XRD spectra of a mixture of Ti and Fe powders MA for different times in argon atmosphere: a) initial state (elemental powder mixture), b) after MA for 2 h, c) after MA for 20 h and d) heat treated at 973 K for 0.5 h

The SEM technique was used to follow the changes in size and shape of the mechanically alloyed powder mixtures as a function of milling time. The microstructure that forms during MA consists of layers of the starting material. The lamellar structure is increasingly refined during further mechanical alloying. The thickness of the material decreases with increase in mechanical alloying time leading to true alloy formation. The sample shows cleavage fracture morphology and inhomogeneous size distribution. Many small powders have a tendency to agglomerate. The size of amorphous powder grains was of the order of 20 nm. The amorphization process of the

Table 1
Properties of studied nanocrystalline alloys

Alloy composition	MA time [h]	Heat treatment [K/h]	Structure	Lattice constants a [nm]	c [nm]	d [nm]	Discharge capacity at 3rd cycle [mAh g^{-1}]
TiFe	20	973/0.5	CsCl	0.2973	–	20	7.50*
$TiFe_{0.25}Ni_{0.75}$	20	973/0.5	CsCl	0.3010	–	–	155**
ZrV_2	25	1073/0.5	$MgCu_2$	0.750	–	35	0*
$Zr_{0.35}Ti_{0.65}V_{0.85}Cr_{0.26}Ni_{1.30}$	30	1073/0.5	$MgZn_2$	0.4921	0.8011	–	260**
$LaNi_5$	30	973/0.5	$CaCu_5$	0.5012	0.3975	25	90**
$LaNi_{3.75}Mn_{0.75}Al_{0.25}Co_{0.25}$	30	973/0.5	$CaCu_5$	0.5075	0.4039	–	255**
Mg_2Ni	90	723/1	Mg_2Ni	0.5216	1.3246	30	100*
$Mg_{1.5}Mn_{0.5}Ni$	90	723/1	Ti_2Ni	1.1321	–	–	241*

d – crystallite size
* – current density of charging and discharging was 4 mA g^{-1}
** – current density of charging and discharging was 40 mA g^{-1}

studied materials was also examined using DSC measurements. XRD studies of MA samples after heating in DSC demonstrated that the observed large exothermic calorimetric effects have to be attributed to the formation of the ordered compounds as a crystallization product.

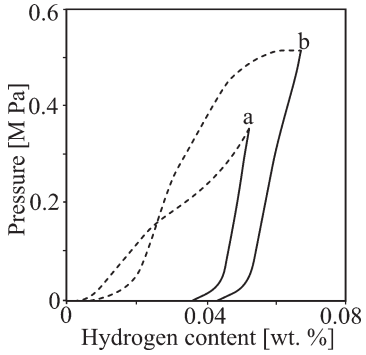

Fig. 3. Electrochemical isotherms pressure-composition for absorption (dashed line) and desorption (solid line) of hydrogen on: a) amorphous, b) nanocrystalline TiFe alloy

The electrochemical pressure-composition (e.p.c.) isotherms for absorption and desorption of hydrogen were obtained from the equilibrium potential values of the electrodes, measured during intermittent charge and/or discharge cycles at constant current density, by using the Nernst equation [26]. Due to the amorphous nature of the studied alloys prior to annealing, the hydrogen absorption-desorption characteristics are not satisfactory. Compared with nanocrystalline TiFe its storage capacity was considerably smaller (Fig. 3). Annealing causes transformation from the amorphous to the crystalline structure and produces grain boundaries. Anani et al. noted that grain boundaries are necessary for the migration of the hydrogen into the alloy [2]. It is worth noting, that the characteristics for polycrystalline and nanocrystalline materials are very similar in respect to hydrogen contents, but there are small differences in the plateau pressures. When the amount of Ni in $TiFe_{1-x}Ni_x$ was increased, the pressure in the plateau region continued to decrease and the hydrogen storage capacity was increased. Pressure-composition isotherms for absorption at room temperature for polycrystalline TiFe and for amorphous FeTi were studied by Zaluski et al. [11]. The hydrogenation behaviour of the amorphous structure was different than that of the thermodynamically stable, crystalline material. For amorphous TiFe material the plateau totally disappears.

Table 2 reports the discharge capacities of the studied polycrystalline, amorphous as well as nanocrystalline TiFe materials. The discharge capacity of electrodes prepared from TiFe alloy powder by application of MA and annealing displayed a very low capacity (7.50 mA h g^{-1} at 4 mA g^{-1} discharge current) whereas the arc melted ones have none [19]. The reduction of the powder size and the creation of new surfaces is effective for the improvement of the hydrogen absorption rate.

Materials obtained when Ni was substituted for Fe in TiFe lead to great improvement in activation behaviour of the electrodes. It was found that the increasing nickel content in $TiFe_{1-x}Ni_x$ alloys leads initially to an increase in discharge capacity, giving a maximum at $x = 0.75$ [20]. In the annealed nanocrystalline $TiFe_{0.25}Ni_{0.75}$ powder, discharge capacity of up to 155 mA h g^{-1} (at 40 mA g^{-1} discharge current) was measured (Fig. 4). The electrodes mechanically alloyed and annealed from the elemental powders displayed the maximum capacities at around the 3-rd cycle but, especially for $x = 0.5$ and 0.75 in $TiFe_{1-x}Ni_x$ alloy, degraded slightly with cycling. This may be due to the easy formation of the oxide layer (TiO_2) during the cycling.

On the other hand, the discharge capacity of nanocrystalline $TiNi_{0.6}Fe_{0.1}Mo_{0.1}Cr_{0.1}Co_{0.1}$ powder has not changed much during cycling (Fig. 4). The alloying elements Mo, Cr and Co, substituted simultaneously for iron atoms in nanocrystalline Ti(Fe-Ni) master alloy have prevented oxidation of this electrode material.

Table 2
Discharge capacities of TiFe alloy prepared by different methods on 3rd cycle (current density of charging and discharging was 4 mA g^{-1})

Microstructure	Processing method	Lattice constant a [nm]	Discharge capacity [mAh g^{-1}]
polycrystalline	arc melting and annealing *	0.2977	0.00
amorphous	MA	–	5.32
nanocrystalline	MA and annealing	0.2973	7.50

* – 1173 K/3 days

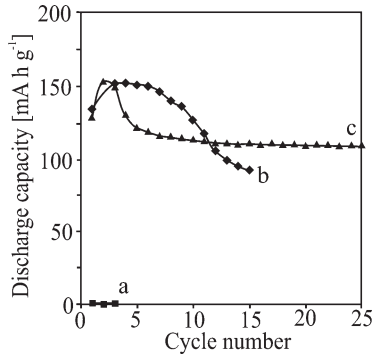

Fig. 4. Discharge capacity as a function of cycle number of electrode prepared with nanocrystalline TiFe (a), $TiFe_{0.25}Ni_{0.75}$ (b) and $TiNi_{0.6}Fe_{0.1}Mo_{0.1}Cr_{0.1}Co_{0.1}$ (c); (solution, 6M KOH; temperature, 293 K). The charge conditions were: 40 mA g^{-1}; The cut-off potential vs. Hg/HgO/6M KOH was −0.7 V

4.2. ZrV_2-type alloys. The nanocrystalline ZrV_2 and $Zr_{0.35}Ti_{0.65}V_{0.85}Cr_{0.26}Ni_{1.30}$ alloys were synthesized by mechanical alloying followed by annealing. The electrochemical properties of nanocrystalline powders were measured and compared to those of amorphous material. The behaviour of MA process has been studied by X-ray diffraction. The powder mixture milled for more than 25 h has transformed absolutely to the amorphous phase. Formation of ordered alloys was achieved by annealing the amorphous materials in high purity argon atmosphere at 1073 K for 0.5 h (Fig. 1b).

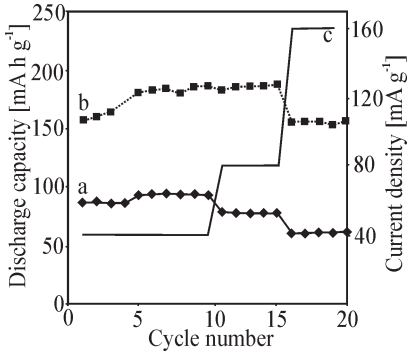

Fig. 5. Discharge capacity as a function of cycle numbers of electrode prepared with (a) amorphous and (b) nanocrystalline $Zr_{0.35}Ti_{0.65}V_{0.85}Cr_{0.26}Ni_{1.30}$ (solution, 6M KOH; temperature, 293 K). The charge conditions were: 40 mA g^{-1}; The discharge conditions were plotted on Figure (c); cut-off potential vs. Hg/HgO/6M KOH was of −0.7 V

Figure 5 shows the discharge capacities of the amorphous and nanocrystalline electrodes as a function of charge/discharge cycling number. The electrode prepared with nanocrystalline $Zr_{0.35}Ti_{0.65}V_{0.85}Cr_{0.26}Ni_{1.30}$ material showed better activation and higher discharge capacities. This improvement is due to a well-established diffusion path for hydrogen atoms along the numerous grain boundaries. Table 3 reports the discharge capacities of the studied ZrV_2-type materials. The electrochemical results show very little difference between the nanocrystalline and polycrystalline powders, as compared with the substantial difference between these and the amorphous powder. In the annealed nanocrystalline $Zr_{0.35}Ti_{0.65}V_{0.85}Cr_{0.26}Ni_{1.30}$ powders prepared by mechanical alloying and annealing discharging capacities up to 150 mA h g^{-1} (at 160 mA g^{-1} discharge current) have been measured [17].

Table 3
Discharge capacities of polycrystalline, amorphous and nanocrystalline $Zr_{0.35}Ti_{0.65}V_{0.85}Cr_{0.26}Ni_{1.30}$ materials (current density of charging and discharging was 160 mA g^{-1})

Preparation method	Structure type	Discharge capacity at 18^{th} cycle [mA h g^{-1}]
arc melting and annealing*	polycrystalline ($MgZn_2$)	135
MA	amorphous	65
MA and annealing	nanocrystalline ($MgZn_2$)	150

* – 1273 K/7 days

Independently, it has been shown, that the electrochemical properties of hydrogen storage alloys, which do not contain nickel, can be stimulated by high-energy ball-milling of the precursor alloys with a small amount of nickel powders [9]. The ZrV_2 and $Zr_{0.5}Ti_{0.5}V_{0.8}Mn_{0.8}Cr_{0.4}$ alloy powders have been prepared using HEBM of precursor alloys with nickel powder. It was confirmed that discharge capacity of electrodes prepared with application of ZrV_2 and $Zr_{0.5}Ti_{0.5}V_{0.8}Mn_{0.8}Cr_{0.4}$ alloy powders with 10 wt% of nickel powder addition was impossible to estimate because of extremely high polarization. In the electrodes prepared with application of high-energy ball-milled ZrV_2/Ni and $Zr_{0.5}Ti_{0.5}V_{0.8}Mn_{0.8}Cr_{0.4}$/Ni alloy powders with 10 wt% of nickel powder the discharge capacities were considerably improved, and they increased from 0 to 110 mA h g^{-1} and 214 mA h g^{-1}, respectively (Table 4).

Table 4
Discharge capacities of nanocrystalline ZrV_2-type materials without and with 10 wt% of Ni powder (current density of charging and discharging was 4 mA g^{-1})

Composition	Discharge capacity [mA h g^{-1}]
ZrV_2	0
ZrV_2/Ni	110
$Zr_{0.5}Ti_{0.5}V_{0.8}Mn_{0.8}Cr_{0.4}$	0
$Zr_{0.5}Ti_{0.5}V_{0.8}Mn_{0.8}Cr_{0.4}$/Ni	214

The alloy elements such as Ti substituted for Zr and Mn, Cr substituted for V in ZrV_2/Ni-based materials greatly improved the activation behaviour of the elec-

trodes. It is worth noting that annealed nanocrystalline ZrV_2/Ni-based powders have greater capacities (about 2.2 times) than the amorphous parent alloy powders. Generally, the electrochemical properties are closely linked to the size and crystallographic perfection of the constituent grains, which in turn are a function of the processing or grain refinement method used to prepare the hydrogen storage alloys.

4.3. $LaNi_5$-type alloys. The properties of hydrogen host $LaNi_5$ materials can be modified substantially by alloying. It was found that the substitution of Ni in $LaNi_5$ by small amounts of Al, Mn, Si, Zn, Cr, Fe, Cu or Co altered the hydrogen storage capacity, the stability of the hydride phase and the corrosion resistance [3]. Generally, in the transition metal sublattice of $LaNi_5$-type compounds, substitution by Mn, Al and Co has been found to offer the best compromise between high hydrogen capacity and good resistance to corrosion [3, 10]. During the MA process originally sharp diffraction lines of La and Ni gradually become broader and their intensity decreases with milling time. The powder mixture milled for more than 30 h has transformed completely to the amorphous phase. Formation of the nanocrystalline alloy was achieved by annealing of the amorphous material in high purity argon atmosphere at 973 K for 0.5 h (Fig. 1c). According to AFM studies, the average size of amorphous La-Ni powders was of order of 25 nm.

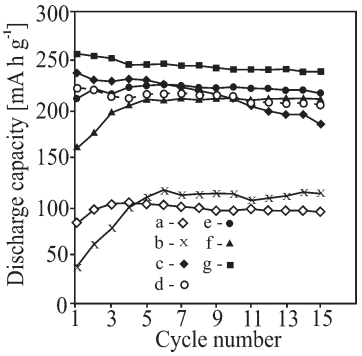

Fig. 6. Discharge capacities as a function of cycle number of $LaNi_5$-type negative electrodes made from nanocrystalline powders prepared by MA followed by annealing: a) $LaNi_5$, b) $LaNi_4Co$, c) $LaNi_4Mn$, d) $LaNi_4Al$, e) $LaNi_{3.75}CoMn_{0.25}$, f) $LaNi_{3.75}CoAl_{0.25}$, g) $LaNi_{3.75}Mn_{0.75}Al_{0.25}Co_{0.25}$ (solution, 6 M KOH; $T = 293$ K). The charge conditions were 40 mA g^{-1}. The cut-off potential vs. Hg/HgO/6 M KOH was −0.7 V

The discharge capacity of an electrode prepared by application of nanocrystalline $LaNi_5$ alloy powder is low (Fig. 6) [22]. It was found that the substitution of Ni by Al or Mn in $La(Ni,M)_5$ alloy leads to an increase in discharge capacity. The $LaNi_4Mn$ electrode, mechanically alloyed and annealed, displayed the maximum capacity at the 1st cycle but discharge capacity degraded strongly with cycling. On the other hand, alloying elements such as Al, Mn and Co substituting nickel greatly improved the cycle life of $LaNi_5$-type material (Fig. 6). With the increase of cobalt content in $LaNi_{4-x}Mn_{0.75}Al_{0.25}Co_x$, the material shows an increase in discharge capacity which passes through a wide maximum for $x = 0.25$ [27]. In nanocrystalline $LaNi_{3.75}Mn_{0.75}Al_{0.25}Co_{0.25}$ discharge capacities up to 258 mA h g^{-1} (at 40 mA g^{-1} discharge current) was measured, which compares with results reported by Iwakura et al. for polycrystalline $MmNi_{4-x}Mn_{0.75}Al_{0.25}Co_x$ alloys (Mm-mishmetal) [28].

Recently the cleanliness of the surface of polycrystalline and nanocrystalline $LaNi_5$-type alloys was studied by X-ray photoelectron spectroscopy (XPS) and Auger electron spectroscopy (AES) [21, 23]. Results showed that the surface segregation under UHV conditions of lanthanum atoms in the mechanically alloyed nanocrystalline samples is significantly stronger compared to that of polycrystalline powders obtained from arc-melted ingots. On the other hand, the level of oxygen impurities trapped in the mechanically alloyed powder during the processing is practically the same as in the arc-melted samples. The substitution of Ni by Al in $LaNi_5$ leads to significant modifications of the electronic structure of the polycrystalline sample. Furthermore, the XPS valence band of the MA nanocrystalline $LaNi_4Al_1$ alloy is considerable broader compared to that measured for the polycrystalline sample. The strong modifications of the electronic structure and the significant surface segregation of lanthanum atoms in the MA nanocrystalline $LaNi_5$-type alloys could significantly influence its hydrogenation properties.

4.4. Mg_2Ni-type alloys. The magnesium-nickel phase diagram shows two compounds Mg_2Ni and $MgNi_2$. The first one reacts with hydrogen slowly at room temperature to form the ternary hydride Mg_2NiH_4. At higher temperatures at pressure (e.g. 473 K, 1.4 MPa [3]), the reaction is rapid enough for useful absorption-desorption reactions to occur.

Mechanical alloying is one of the approaches to produce Mg-Ni alloys which have been highly expected to be used as hydrogen storage materials [29]. Ling et al. [30] pointed out that HEBM which gives rise to the creation of fresh surfaces and cracks is highly effective for the kinetic improvement in initial hydriding properties.

In this work, the nanocrystalline Mg_2Ni-type alloys were prepared by mechanical alloying followed by annealing. The powder mixture milled for more than 90 h has transformed completely to the amorphous phase, without formation of another phase. Formation of the nanocrystalline alloy was achieved by annealing of the amorphous material in high purity argon atmosphere at 723 K for 0.5 h. All diffraction peaks were assigned to those of the hexagonal crystal structure with cell parameters $a = 0.5216$ nm, $c = 1.3246$ nm (Fig. 1d) [13]. According to AFM studies, the average size of amorphous Mg-Ni powders was of the order of 30 nm.

At room temperature, the nanocrystalline Mg_2Ni alloy absorbs hydrogen, but almost does not desorb

it. At temperatures above 523 K the kinetic of the absorption-desorption process improves considerably and for nanocrystalline Mg_2Ni alloy the reaction with hydrogen is reversible. The hydrogen content in this material at 573 K is 3.25 wt%. Upon hydrogenation, Mg_2Ni transforms into the hydride Mg_2NiH_x phase. It is important to note, that between 518–483 K the hydride Mg_2NiH_x phase transforms from a high temperature cubic structure to a low temperature monoclinic phase. When hydrogen is absorbed by Mg_2Ni beyond 0.3 H per formula unit, the system undergoes a structural rearrangement to the stoichiometric complex Mg_2NiH_x hydride, with an accompanying 32% increase in volume. The electrochemical properties of the alloy are improved after substitution of some amounts of magnesium by manganese. The results show that the maximum absorption capacity reaches 3.25 wt% for pure nanocrystalline Mg_2Ni alloy. This is lower than the polycrystalline Mg_2Ni alloy (3.6 wt% [10]) due to a significant amount of strain, chemical disorder and defects introduced into the material during the mechanical alloying process [11]. At the same time, increasing manganese substitution causes the unit cell to decrease. The concentration of hydrogen in produced nanocrystalline Mg_2Ni alloys strongly decreases with increasing Mn contents. The hydrogen content at 573 K in nanocrystalline $Mg_{1.5}Mn_{0.5}NiH$ was only 0.65 wt%.

The Mg_2Ni electrode, mechanically alloyed and annealed, displayed the maximum discharge capacity (100 mA h g^{-1}) at the 1st cycle but degraded strongly with cycling. The poor cyclic behaviour of Mg_2Ni electrodes is attributed to the formation of $Mg(OH)_2$ on the electrodes, which has been considered to arise from the charge-discharge cycles [31]. To avoid the surface oxidation, we have examined the effect of magnesium substitution by Mn or Al in Mg_2Ni-type material. This alloying greatly improved the discharge capacities. In nanocrystalline $Mg_{1.5}Mn_{0.5}Ni$ and $Mg_{1.5}Al_{0.5}Ni$ alloys discharge capacities up to 241 mA h g^{-1} and 175 mA h g^{-1} were measured, respectively [13].

The surface chemical composition of nanocrystalline Mg_2Ni-type alloy studied by X-ray photoelectron spectroscopy (XPS) showed the strong surface segregation under UHV conditions of Mg atoms in the MA nanocrystalline Mg_2Ni alloy. This phenomenon could considerably influence the hydrogenation process in such a type of materials, as well.

4.5. Composite-type nanomaterials. A new class of electrode materials, composite hydride materials, is proposed for anodes in hydride based rechargeable batteries [32, 33]. These materials were synthesized by mechanical mixing of two components: a major component having good hydrogen storage properties and a minor component used us surface activator. The major component was selected among conventional hydride electrode materials; alloys of the TiFe-, ZrV_2-, $LaNi_5$- and Mg_2Ni-type type. The minor component was usually nickel or graphite. Till now, the composite hydride electrodes using Ni as minor component have shown the following advantages: almost a complete elimination of the need for initial activation, an enhancement of the discharge capacity, a considerable improvement in the stability to charge/discharge at high rates, an increase in the charging efficiency, a higher resistance to surface degradation during repeated charge/discharge.

In order to improve the electrochemical properties of the studied so far nanocrystalline electrode materials, the ball-milling technique was applied to the TiFe- and Mg_2Ni-type alloys using the nickel and graphite elements as surface modifiers [34, 35]. The $TiFe_{0.25}Ni_{0.75}$/M- and $Mg_{1.5}Mn_{0.5}Ni$/M-type composite materials, where M = 10 wt% Ni or C, were produced by ball–milling for 1 h and 30 min, respectively. Ball–milling with nickel or graphite of $TiFe_{0.25}Ni_{0.75}$- and $Mg_{1.5}Mn_{0.5}Ni$-type materials is sufficient to considerably broaden the diffraction peaks of $TiFe_{0.25}Ni_{0.75}$ and $Mg_{1.5}Mn_{0.5}Ni$ (not shown). Additionally, milling with graphite is responsible for a sizeable reduction of the crystallite sizes of $TiFe_{0.25}Ni_{0.75}$/C and $Mg_{1.5}Mn_{0.5}Ni$/C from 30 nm to 20 nm.

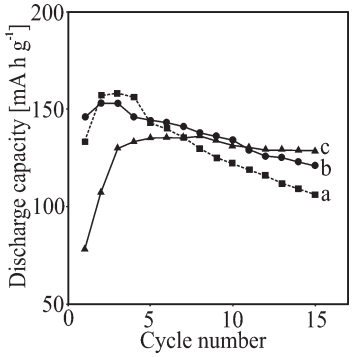

Fig. 7. The discharge capacity as a function of cycle number for MA and annealed $TiFe_{0.25}Ni_{0.75}$ (a) as well as $TiFe_{0.25}Ni_{0.75}$/Ni (b) and $TiFe_{0.25}Ni_{0.75}$/C (c) composite electrodes (solution, 6 M KOH; temperature, 293 K)

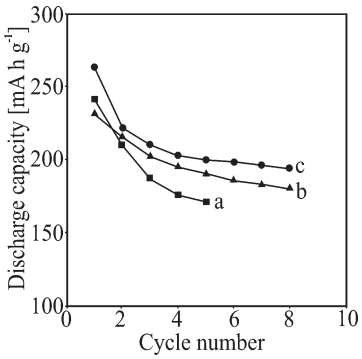

Fig. 8. The discharge capacity as a function of cycle number for MA and annealed $Mg_{1.5}Mn_{0.5}Ni$ (a) as well as $Mg_{1.5}Mn_{0.5}Ni$/Ni (b) and $Mg_{1.5}Mn_{0.5}Ni$/C (c) composite electrodes (solution, 6 M KOH; temperature, 293 K)

Figures 7 and 8 show the discharge capacities as a function of the cycle number for studied nanocomposite materials. When coated with nickel, the discharge capacities of nanocrystalline $TiFe_{0.25}Ni_{0.75}$ and $Mg_{1.5}Mn_{0.5}Ni$ powders were increased. The elemental nickel was distributed on the surface of ball milled alloy particles homogenously and role of these particles is to catalyse the dissociation of molecular hydrogen on the surface of studied alloy. Mechanical coating with nickel or graphite effectively reduced the degradation rate of the studied electrode materials. Compared to that of the uncoated powders, the degradation of the coated was suppressed. Recently, Raman and XPS investigations indicated the interaction of graphite with MgNi alloy occurred at the Mg part in the alloy [36]. Graphite inhibits the formation of new oxide layer on the surface of materials once the native oxide layer is broken during the ball–milling process.

5. Electronic properties

Application of hydrogen storage alloys as anode materials focused attention also on the electronic structure of TiFe, ZrV_2, $LaNi_5$ or Mg_2Ni and its modification mainly by Ni atoms but also by Al, Co, Cr and Mo impurities [37–45]. In order to optimise the choice of the compounds for an electrochemical application, a better understanding of the role of each alloy constituent on the electronic properties of the material is crucial. Several semi-empirical models [46, 47] for the heat of formation and heat of solution of metal hydrides have been proposed and attempts for justifying the maximum hydrogen absorption capacity of the metallic matrices have been made. These models showed that the energy of the metal-hydrogen interaction depends both on geometric and electronic factors.

Recently, the electronic structure of Ti-based systems was studied by the tight-binding version of the linear muffin-tin method in the atomic sphere approximation (TB–LMTO ASA) [39]. In the $TiFe_{1-x}Ni_x$ alloys, increasing the content of the Ni impurities extended the valence bands and increased the density of states at the Fermi level. Similar effects were observed for the $TiNi_{0.6}Fe_{0.1}Mo_{0.1}Cr_{0.1}Co_{0.1}$ system.

Independently, the electronic properties of polycrystalline and nanocrystalline $TiFe_{0.25}Ni_{0.75}$ alloys were studied using X-ray photoelectron spectroscopy (XPS) [40]. In general, the lattice expansion associated with Fe substitution by Ni in $TiFe_{1-x}Ni_x$ could cause a narrowing of the Ni-d subband due to a decrease in the Ni-Ni interaction. The above effect is manifested as a relatively sharp maximum of the valence band [40]. Furthermore, the experimental valence band could be also broader due to the effect of disorder caused by substitution of Fe by Ni. The shape of the XPS valence band of the nanocrystalline $TiFe_{0.25}Ni_{0.75}$ alloy is broader compared to that measured for the polycrystalline $TiFe_{0.25}Ni_{0.75}$ sample. This is probably due to a strong deformation of the nanocrystals. Normally the interior of the nanocrystal is constrained and the distances between atoms located at the grain boundaries are expanded. Furthermore, in the case of MA nanocrystalline $TiFe_{0.25}Ni_{0.75}$ alloy the Ni atoms could also occupy metastable positions in the deformed grain. The above behaviour could also modify the electronic structure of the valence band.

The electronic structure of $Zr(V\text{-}Ni)_2$-type compounds has also been studied [42]. The Ni impurities cause a charge transfer from the Zr and V atoms to the Ni atom, the valence band is wider and the density of electronic states at the Fermi level decreases by about 30%.

Recently, the effect of the substitution at the Ni site on the electronic structure of $LaNi_5$-type compounds was investigated [43, 44]. It was found as a very good agreement between experimental results and ab-initio LMTO calculations of the total density of states (DOS) [43]. The occupied part of the conduction band is dominated by the Ni-3d states with a non-negligible bonding contribution of the La-5d states. The main part of the La-5d states is located above the Fermi energy [44]. The XPS signal at E_F is high and mostly composed of Ni-3d states since the La-5d contribution is practically negligible [43].

The XPS valence band spectrum of polycrystalline $LaNi_4Al$ is significantly modified compared to that measured for the $LaNi_5$. In general, the lattice expansion associated with nickel substitution by aluminium could cause a narrowing of the Ni-3d subband due to a decrease in the Ni-Ni interaction. The above effect is manifested as a relatively sharp maximum of the valence band. On the other hand, the width of the valence band of the $LaNi_4Al_1$ alloy is greater in comparison with $LaNi_5$ system. This is due to the contribution of the Al s and p subbands, which are located near the bottom of the total valence band [43]. Furthermore, the experimental valence band could be also broader due to the effect of disorder caused by substitution of Ni by Al. Additionally, the XPS valence band of the nanocrystalline $LaNi_4Al_1$ alloy is broader compared to that measured for the polycrystalline $LaNi_4Al_1$ sample [45].

Binary $LaNi_5$ crystallises with the $CaCu_5$ structure type in which La occupies site 1(a) and Ni sites 2(c) and 3(g). The battery electrode material $LaNi_4Al_1$ is a substitutional derivative of $LaNi_5$ in which La occupies site 1(a) and Ni and Al sites 2(c) and 3(g) of space group P6/mmm. Experimental results showed that the La sites do not accommodate Ni and Al atoms. Furthermore, TB LMTO calculation [43] showed that the impurity aluminium atoms prefer the 3g positions in agreement with experimental data [48]. However, in the case of MA nanocrystalline $LaNi_4Al_1$ alloy the Al atoms could also occupy metastable (2c) positions in the deformed grain. The above behaviour could also modify the electronic structure of the valence band.

A large number of experimental investigations on Mg-Ni compounds have been performed up to now in relation

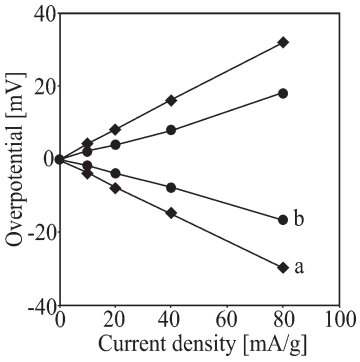

Fig. 9. Overpotential against current density on activated nanocrystalline: (a) $TiFe_{0.25}Ni_{0.75}$; and (b) TiNi electrodes, at 15 s of anodic and cathodic galvanostatic pulses

to their electrochemical properties [11–13]. The band structure calculations were performed for ideal hexagonal Mg_2Ni type structure with $P6_222$ space group. In this structure magnesium and nickel atoms each occupied two crystallographic positions: Mg(6i), Mg(6f), Ni(3d), and Ni(3b). Our total energy calculations showed that in both cases, $Mg_{11/6}Al_{1/6}Ni$ and $Mg_{11/6}Mn_{1/6}Ni$, the impurity atoms, Al and Mn, prefer (6i) position. Al atoms modify bottom of the valence band, which is by about 0.5 eV wider than for Mg_2Ni system. In the case of Mn atoms, 4d electrons modify valence band in the range of 3 eV below the Fermi level (E_F), the value of DOS for $E = E_F$ is higher [25].

The experimental XPS valence bands for nanocrystalline Mg_2Ni and $Mg_{1.5}Mn_{0.5}Ni$ were studied. Similarly to the effect of the band broadening observed for the nanocrystalline TiFe and $LaNi_5$ based alloys, we have observed such a modification in the case of the Mg_2Ni system. The reasons responsible for the band broadening of the nanocrystalline Mg_2Ni are the same as already described above for the nanocrystalline TiFe- and $LaNi_5$-type alloys. We believe that also in the case of the nanocrystalline $Mg_{1.5}Mn_{0.5}Ni$ system its experimental valence band is broadened compared to that for a polycrystalline alloy.

The present theoretical studies will hopefully stimulate further experimental investigations which lead to a full understanding of the electronic properties of these technologically important hydrogen storage materials.

6. Closed cells

The cyclic behaviour of the some nanocrystalline TiFe-type alloy anodes was examined in a sealed HB 116/054 cell (according to the International standard IEC no. 61808, related to the hydride button rechargeable single cell) [49]. The mass of the active material was 0.33 g. To prepare MH negative electrodes, alloy powders were mixed with addition of 5 wt.% tetracarbonylnickel. Then this mixture was pressed into the form tablets which were placed in a small basket made of nickel nets (as the current collector). The diameter of each tested button cells was 6.6 mm and a thickness of 2.25 mm, respectively. The sealed Ni-MH cell was constructed by the pressing negative and positive electrode, polyamide separator and KOH ($\rho = 1.20 \cdot 10^{-3}$ kg m^{-3}) as electrolyte solution. The battery with electrode fabricated from nanocrystalline materials was charged at current density of $i = 3$ mA g^{-1} for 15 h and after 1 h pause discharged at current density of $i = 7$ mA g^{-1} down to 1.0 V. All electrochemical measurements were performed at 293 ± 1 K.

To study the quality of the actived $TiFe_{0.25}Ni_{0.75}$ and TiNi as electrode materials in the Ni-MH battery, the overpotential dependence on the current density ($i = 10$, 20, 40 and 80 mA g^{-1}) was recorded at 15 s of anodic and cathodic galvanostatic pulses (Fig. 9). It can be see that the anodic and cathodic parts of nanocrystalline electrodes are almost symmetrical with respect to the rest potential of the electrode. It may be concluded that for all studied electrodes fast rates can be achieved.

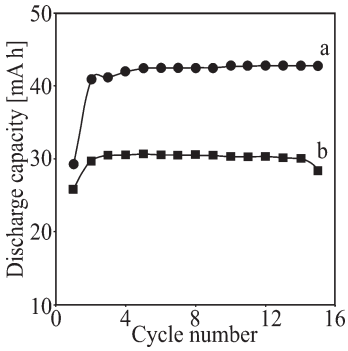

Fig. 10. Durability of the sealed button cells with negative electrodes made from nanocrystalline: a) $TiFe_{0.25}Ni_{0.75}$ and b) TiNi alloys (the mass of the active material was 0.33 g)

Figure 10 shows the discharge capacities of sealed button cells with electrodes prepared from nanocrystalline $TiFe_{0.25}Ni_{0.75}$ and TiNi alloys as a function of discharge cycle number. The electrode and sealed battery using the nanocrystalline $TiFe_{0.25}Ni_{0.75}$ alloy show better characteristics than that using the nanocrystalline TiNi alloy. The results show that the sealed battery using the nanocrystalline $TiFe_{0.25}Ni_{0.75}$ alloy has the capacity of the polycrystalline $(Zr_{0.35}Ti_{0.65})(V_{0.93}Cr_{0.28}Fe_{0.19}Ni_{1.0})$ one [7, 50].

Recently, it was found that the discharge capacities of sealed button cells with electrodes prepared from the nanocrystalline $La(Ni,Mn,Al,Co)_5$ powders had a slightly higher discharge capacities, compared with negative electrodes prepared from polycrystalline powders [51].

7. Conclusion

In conclusion, nanocrystalline TiFe-, ZrV_2-, $LaNi_5$- and Mg_2Ni-type alloys synthesized by mechanical alloying can reversibly store hydrogen to form hydride and release hydrogen electrochemically. The hydrogen storage properties of nanocrystalline ZrV_2- and $LaNi_5$-type powders prepared by mechanical alloying and annealing show no

big difference with those of melt casting (polycrystalline) alloys. On the other hand, the nanocrystalline TiFe- and Mg_2Ni-type hydrides show substantially enhanced absorption characteristics superior to those of the conventionally prepared materials. The properties of nanocrystalline electrode were attributed to the structural characteristics of the compound caused by mechanical alloying. Mechanical alloying is a suitable procedure for obtaining nanocrystalline hydrogen storage materials with high capacities and better hydrogen sorption properties. At present, the Ni-MH battery is a key component for advanced information and telecommunication systems. The input materials for this high-tech battery would be nanocrystalline hydrogen storage alloys.

Acknowledgements. The financial support of the Polish National Committee for Scientific Research (KBN) under the contracts No: KBN–7 T08D 015 12 (1997–2000), PBZ/KBN–013/T08/02 (2000–2003) and KBN–8 T10A 001 20 (2001–2004) is gratefully acknowledged. The author would also like to extend his appreciation to dr E. Jankowska and dr W. Majchrzycki, former PhD students, from Central Laboratory of Batteries and Cells (CLAiO) Poznań for electrochemical measurements. Special thanks to dr J. Jakubowicz, dr M. Nowak and dr K. Smardz, Poznań University of Technology; dr L. Smardz and dr A. Szajek, Institute of Molecular Physics, Polish Academy of Sciences for their contributions to various aspects of the work reported.

References

[1] G. Sandrock, "A panoramic overview of hydrogen storage alloys from a gas reaction point of view", *J. Alloys Comp.* 293–295, 877–888 (1999).

[2] A. Anani, A. Visintin, K. Petrov, S. Srinivasan, J. J. Reilly, J. R. Johnson, R. B. Schwarz and P. B. Desch, "Alloys for hydrogen storage in nickel/hydrogen and nickel/metal hydride batteries", *J. Power Sources* 47, 261–275 (1994).

[3] J. Kleparis, G. Wojcik, A. Czerwinski, J. Skowronski, M. Kopczyk and M. Beltowska-Brzezinska, "Electrochemical behavior of metal hydrides", *J. Solid State Electrochem.* 5, 229–249 (2001).

[4] M. Jurczyk, "Nanocrystalline metal hydride electrode materials", *Current Topics in Electrochem.* 9, 105–116 (2003).

[5] M. Jurczyk, L. Smardz, M. Makowiecka, E. Jankowska and K. Smardz, "The synthesis and properties of nanocrystalline electrode materials by mechanical alloying", *J. Phys. Chem. Sol.* 65, 545–548 (2004).

[6] K. H. J. Buschow, P. C. P. Bouten and A. R. Miedema, "Hydrides formed from intermetallic compounds of two transition metals: a special class of ternary alloys", *Rep. Prog. Phys.* 45, 937–1039 (1982).

[7] K. Hong, "The development of hydrogen storage alloys and the progress of nickel hydride batteries", *J. Alloys Comp.* 321, 307–313 (2001).

[8] M. Jurczyk, W. Rajewski, G. Wojcik and W. Majchrzycki, "Metal hydride electrodes prepared by mechanical alloying of ZrV_2-type materials", *J. Alloys Comp.* 285, 250–254 (1999).

[9] M. Jurczyk, W. Rajewski, W. Majchrzycki and G. Wojcik, "Synthesis and electrochemical properties of high energy ball milled Laves phase $(Zr,Ti)(V,Mn,Cr)_2$ alloys with nickel powder", *J. Alloys Comp.* 274, 299–302 (1998).

[10] T. Sakai, M. Matsuoka and C. Iwakura, in: *Handbook on the Physics and Chemistry of Rare Earth*, Vol. 21, Chapter 142, K.A. Gschneider Jr., L. Eyring (Eds.), Amsterdam: Elsevier Science B.V., 1995.

[11] L. Zaluski, A. Zaluska and J. O. Ström-Olsen, "Nanocrystalline metal hydrides", *J. Alloys Comp.* 253-254, 70–79 (1997).

[12] S. Orimo, A. Zttel, K. Ikeda, S. Saruki, T. Fukunaga, H. Fujii and L. Schlapbach, "Hydriding properties of the MgNi-based systems", *J. Alloys Comp.* 293-295, 437–442 (1999).

[13] A. Gasiorowski, W. Iwasieczko, D. Skoryna, H. Drulis and M. Jurczyk, "Hydriding properties of nanocrystalline $Mg_{2-x}M_xNi$ alloys synthesised by mechanical alloying (M = Mn, Al)", *J. Alloys Comp.* 364, 283–288 (2004).

[14] G. Giang, J. Huot and R. Scultz, "Hydrogen storage properties of the mechanically alloyed $LaNi_5$-based materials", *J. Alloys Comp.* 320, 133–139 (2001).

[15] J. S. Benjamin, "Mechanical alloying", *Sc. American.* 234, 40–57 (1976).

[16] C. Suryanarayna, "Mechanical alloying", *Progr. Mater. Sc.* 46, 1–184 (2001).

[17] W. Majchrzycki and M. Jurczyk, "Electrode characteristics of nanocrystalline $(Zr,Ti)(V,Cr,Ni)_{2.41}$ compound", *J. Power Sources* 93, 77–81 (2001).

[18] E. Jankowska and M. Jurczyk, "Electrochemical behaviour of high-energy ball-milled TiFe alloy", *J. Alloys Comp.* 346, L1–L3 (2002).

[19] M. Jurczyk, E. Jankowska, M. Nowak and I. Wieczorek, "Electrode characteristics of nanocrystalline TiFe-type alloys", *J. Alloys Comp.* 354, L1–L4 (2003).

[20] M. Jurczyk, E. Jankowska, M. Nowak and J. Jakubowicz, "Nanocrystalline titanium type metal hydrides prepared by mechanical alloying", *J. Alloys Comp.* 336, 265–269 (2002).

[21] M. Jurczyk, K. Smardz, W. Rajewski and L. Smardz, "Nanocrystalline $LaNi_{4.2}Al_{0.8}$ prepared by mechanical alloying and annealing and its hydride formation", *Mater. Sc. Eng.* A303, 70–76 (2001).

[22] M. Jurczyk, M. Nowak, E. Jankowska and J. Jakubowicz, "Structure and electrochemical properties of the mechanically alloyed $La(Ni,M)_5$ materials", *J. Alloys Comp.* 339, 339–343 (2002).

[23] L. Smardz. K. Smardz, M. Nowak and M. Jurczyk, "Structure and electronic properties of $La(Ni,Al)_5$ alloys", *Cryst. Res. & Technology* 36, 1385–1392 (2001).

[24] M. Jurczyk, L. Smardz, K. Smardz, M. Nowak and E. Jankowska, "Nanocrystalline $LaNi_5$-type electrode materials for Ni-MH_x batteries", *J. Solid State Chem.* 171, 30–37 (2003).

[25] M. Jurczyk, L. Smardz and A. Szajek, "Nanocrystalline materials for NiMH batteries", *Mat. Sc. Eng. B* 108, 67–75 (2004).

[26] M. Kopczyk, G. Wojcik, G. Mlynarek, A. Sierczynska and M. Beltowska-Brzezinska, "Electrochemical absorption-desorption of hydrogen on multicomponent Zr-Ti-V-Ni-Cr-Fe alloys in alkaline solution", *J. Appl. Electrochem.* 26, 639–645 (1996).

[27] M. Jurczyk, M. Nowak and E. Jankowska, "Nanocrystalline $LaNi_{4-x}Mn_{0.75}Al_{0.25}Co_x$ electrode materials produced by mechanical alloying", *J. Alloys Comp.* 340, 281–285 (2002).

[28] C. Iwakura, K. Fukuda, H. Senoh, H. Inoue, M. Matsuoka and Y. Yamamoto, "Electrochemical characterization of $MmNi_{4.0-x}Mn_{0.75}Al_{0.25}Co_x$ electrodes as a function of cobalt content", *Electrochim. Acta* 43, 2041–2046 (1998).

[29] L. Aymard, M. Ichitsubo, K. Uchida, E. Sekreta and F. Ikazaki, "Preparation of Mg_2Ni base alloy by the combination of mechanical alloying and heat treatment at low temperature", *J. Alloys Comp.* 259, L5–L8 (1997).

[30] G. Ling, S. Boily, J. Huot, A. Van Neste and R. Schultz, "Hydrogen absorption properties on a mechanically milled Mg-50 wt.% $LaNi_5$ composite", *J. Alloys Comp.* 268, 302–307 (1998).

[31] D. Mu, Y. Hatano, T. Abe and K. Watanabe, "Degradation kinetics of discharge capacity for amorphous Mg–Ni electrode", *J. Alloys Comp.* 334, 232–237 (2002).

[32] S. Bouaricha, J. P. Dodelet, D. Guay, J. Huot and R. Schultz, "Activation characteristics of graphite modified hydrogen absorbing materials", *J. Alloys Comp.* 325, 245–251 (2001).

[33] J. Chen, D. H. Bradhurst, S. X. Don and H. K. Liu, "The effect of chemical coating with Ni on the electrode properties of Mg_2Ni alloys", *J. Alloys Comp.* 280, 290–293 (1998).

[34] M. Jurczyk, "Nanostructured electrode materials for Ni-MH_x batteries prepared by mechanical alloying", *J. Mater. Science* (2004), to be published.

[35] M. Makowiecka, D. Skoryna and M. Jurczyk, "Nanocrystalline TiNi-type electrode materials for Ni-MH batteries", *Inżynieria Materiałowa* (2004), to be published.

[36] C. Iwakura, H. Inoue, S. G. Zhang and S. Nohara, "A new electrode material for nickel-metal hydride batteries: MgNi–graphite composites prepared by ball-milling", *J. Alloys Comp.* (293–295), 653–657 (1999).

[37] M. Gupta, "Electronic structure of TiFeH", *J. Phys. F: Metal Phys.* 12, L57–62 (1982).

[38] G. N. Garcia, J. P. Abriata and J. O. Sofo, "Calculation of the electronic and structural properties of cubic Mg_2NiH_4", *Phys. Rev.* B59, 11746–11754 (1999).

[39] A. Szajek, M. Jurczyk and E. Jankowska, "The electronic and electrochemical properties of the TiFe-based alloys", *J. Alloys Comp.* 348, 285–292 (2003).

[40] K. Smardz, L. Smardz, M. Jurczyk and E. Jankowska, "Electronic properties of nanocrystalline and polycrystalline $TiFe_{0.25}Ni_{0.75}$ alloys", *Phys. Stat. Sol. (a)* 196, 263–266 (2003).

[41] A. Szajek, M. Jurczyk and E. Jankowska, "The electronic and electrochemical properties of the $TiFe_{1-x}Ni_x$ alloys", *Phys. Stat. Sol.* 196, 256–259 (2003).

[42] A. Szajek, M. Jurczyk and W. Rajewski, "The electronic and electrochemical properties of the ZrV_2 and $Zr(V_{0.75}Ni_{0.25})_2$ systems", *J. Alloys Comp.* 302, 299–303 (2000).

[43] A. Szajek, M. Jurczyk and W. Rajewski, "The electronic structure and electrochemical properties of the $LaNi_5$, $LaNi_4Al$ and $LaNi_3AlCo$ systems", *J. Alloys Comp.* 307, 290–296 (2000).

[44] L. Smardz, K. Smardz, M. Nowak and M. Jurczyk, "Structure and electronic properties of $La(Ni,Al)_5$ alloys", *Cryst. Res. & Techn.* 36, 1385–1392 (2001).

[45] A. Szajek, M. Jurczyk, M. Nowak and M. Makowiecka, "The electronic and electrochemical properties of the $LaNi_5$-based alloys", *Phys. Stat. Sol. (a)* 196, 252–255 (2003).

[46] R. Griessen, "Heats of solution and lattice-expansion and trapping energies of hydrogen in transition metals", *Phys. Rev.* B38, 3690–3698 (1988).

[47] P. C. Bouten and A. R. Miedema, "On the heats of formation of the binary hydrides of transition metals", *J. Less Common Metals* 71, 147–151 (1980).

[48] J. M. Joubert, M. Latroche, A. Percheron-Guégan and F. B. Bourée-Vigueron, "Thermodynamic and structural comparison between two potential metal-hydride battery materials $LaNi_{3.55}Mn_{0.4}Al_{0.3}Co_{0.75}$ and $CeNi_{3.55}Mn_{0.4}Al_{0.3}Co_{0.75}$", *J. Alloys Comp.* (275–277), 118–122 (1998).

[49] E. Jankowska and M. Jurczyk, "Electrochemical properties of sealed Ni-MH batteries using nanocrystalline TiFe-type anodes", *J. Alloys Comp.* 372, L9–L12 (2004).

[50] J. M. Skowronski, A. Sierczynska and M. Kopczyk, "Investigation of the influence of nickel content on the correlation between the hydrogen equilibrium pressure for hydrogen absorbing alloy and the capacity of MH electrodes in open and closed cells", *J. Solid State Electrochem.* 7, 11–16 (2002).

[51] unpublished results